Ionics (2022) 28:2125–2133
https://doi.org/10.1007/s11581-022-04458-x

ORIGINAL PAPER

Regenerated $LiFePO_4$/C for scrapped lithium iron phosphate powder batteries by pre-oxidation and reduction method

Hao Zhang[1] · Lihua Wang[2] · Yongzhi Chen[2] · Xu Wen[2]

Received: 30 July 2021 / Revised: 11 January 2022 / Accepted: 14 January 2022 / Published online: 12 February 2022

Abstract

The cathode materials of scrapped lithium-iron phosphate battery are mainly composed of $LiFePO_4$/C, conductive agent and PVDF, etc. Unreasonable disposal will cause serious environmental pollution and waste of scarce resources. In this paper, cathode materials were regenerated by pre-oxidation and reduction method. Impurities such as carbon coating, conductive agent, and PVDF were removed and $LiFePO_4$/C was converted to Fe_2O_3 and $Li_3Fe_2(PO_4)_3$ by pre-oxidation. After the addition of sucrose, regenerated$LiFePO_4$/C was synthesized under reduction process. The effects of calcination temperature and sucrose addition on the microstructure and electrochemical properties of regenerated $LiFePO_4$/C were studied. The regenerated $LiFePO_4$/C had excellent cycling stability when the sucrose addition was 12% and calcined at 700 ℃. The initial discharge specific capacity of regenerated $LiFePO_4$/C was 145.51 mAh g^{-1} at 0.5 C. After 200 cycles, the discharge specific capacity was 145.25 mAh g^{-1} (capacity retention rate: 99.82%). It provides a new inspiration for the high-value recycling and regeneration of the other scrapped lithium-ion batteries.

Keywords Scrapped lithium-ion batteries · Regenerated $LiFePO_4$/C · Pre-oxidation and reduction

Introduction

In recent years, the establishment of a green and low-carbon energy system has become the consensus in the world, and some countries have reduced carbon emissions by accelerating the development of electric vehicles (EVs) [1]. Lithium-iron phosphate power batteries (LFPBs) are widely used in energy storage [2], pure electric vehicle (PEV) [3, 4], and hybrid electric vehicle (HEVs) [5], etc., due to their advantages such as good safety, long cycle life, and abundant raw materials. As battery production increases, the number of LFPBs decommissioned gradually increases. The scrapped cathode materials of LFPBs are mainly composed of $LiFePO_4$/C, conductive carbon black, and PVDF, etc. [6]. Unreasonable disposal will cause serious environmental pollution and resource waste [7, 8].

In the past studies, hydrometallurgy technology was widely used for the recycling and regeneration of scrapped $LiFePO_4$/C [9]. Hydrometallurgical technology mainly uses acid, alkali, and other solutions to dissolve the material, and then the corresponding lithium salt, iron salt, and phosphate salt were obtained by precipitation and purification method. Lithium salt, iron salt, and phosphate were mixed in proportions and then added to the carbon source for calcination to obtain regenerated $LiFePO_4$/C [10, 11]. The $LiFePO_4$/C prepared by metallurgical method had high purity, controllable morphology, and grain size [12]. However, the pollution is great and the preparation process is complicated [13, 14].

The direct regeneration technology of scrapped $LiFePO_4$/C has the advantages of simple process and small environmental pollution [15, 16]. Li [17] and Chen [18] et al. added Li_2CO_3 (lithium source) into the scrapped $LiFePO_4$/C and mixed it uniformly to obtain the regenerated $LiFePO_4$/C with good physicochemical and electrochemical properties by calcination. In order to reduce the content of impurities in regenerated $LiFePO_4$/C, Yang et al. [19] used DMAC to separate Al foil from scrapped cathode plates and the scrapped $LiFePO_4$/C with high purity was

✉ Lihua Wang
csuwanglihua@csu.edu.cn

✉ Yongzhi Chen
mitaer113@csu.edu.cn

[1] College of Mechanical and Electrical Engineering, Changsha University, Changsha 410022, China

[2] College of Mechanical Engineering, Hunan Institute of Science and Technology, Yueyang 414006, China

obtained. However, the carbon coating in the regenerated $LiFePO_4$/C obtained by direct regeneration technology had many damages, and the crystal lattice of $LiFePO_4$ still had many defects. It made the electrochemical performance of regenerated $LiFePO_4$/C poor.

In this paper, the scrapped $LiFePO_4$/C was regenerated by pre-oxidation and reduction method. The impurities such as carbon coating, conductive agent, and binder in scrapped $LiFePO_4$/C were removed by pre-oxidation calcination, and the mixture of Fe_2O_3 and $Li_3Fe_2(PO_4)_3$ was obtained. The $LiFePO_4$/C was synthesized by the reduction of amorphous carbon in Ar atmosphere. The regenerated $LiFePO_4$/C had a complete carbon coating, few lattice defects, and excellent electrochemical performance. This study could provide experimental basis for the preparation of high-performance regenerated $LiFePO_4$/C.

Experiment

Material preparation

The scrapped LFPBs were disassembled and separated to obtain the cathode plates. During the battery cycle, the repeated heating of binder and collector will lead to the failure of binder. This will reduce the ion exchange efficiency between the cathode materials and the collector, resulting in the degradation of electrochemical performance. In order to make the binder ineffective and then obtain the scrapped cathode materials, the scrapped cathode plates were calcined at 300 ℃ for 1 h in air atmosphere then removed the aluminum foil. The scrapped cathode materials were calcined in the air again at 600 ℃ for 20 min. The color of scrapped cathode materials changed from black to brick red, and the mixtures were mainly composed of Fe_2O_3 and $Li_3Fe_2(PO_4)_3$ [20]. Sucrose was added to the mixtures and homogenized by milling with zirconia balls in polyethylene containers for 6 h. The mixtures were calcined at 500–750 ℃ for 3 h in high-purity Ar atmosphere. The chemical reaction that occurs during heat treatment is as follow:

$$Li_3Fe_2(PO_4)3 + Fe_2O_3 + C_{12}H_{22}O_{11} \rightarrow LiFePO_4 + C + CO_2(gas) + H_2O\ (gas)$$

Materials characterization

The crystallite structures of the samples were characterized by X-ray diffraction (XRD) (D / Max 2550, Rigaku) using Cu Kα radiation operated at 18 Kw. The structural characteristics of the samples were investigated by field-emission scanning electron microscopy (SEM) (MIRA 3 LMU, Tescan) and high-resolution transmission electron microscopy (HRTEM) (G2 F20, Tecnai).

Electrochemical measurement

The cathode electrodes were fabricated by forming slurry of the active materials, Super C, and polyvinylidene fluoride (PVDF) in N-methyl-2-pyrrolidinone (NMP) at a weight ratio of 92:4:4. The prepared homogeneous slurry was coated onto aluminum foil and dried at 100 °C for 30 min. The cathode, separator, lithium plate, and electrolyte were combined to make 2032 cells. The electrolyte was 1 M $LiPF_6$ dissolved in the mixture of diethyl carbonate (DEC), dimethyl carbonate (DMC), and ethylene carbonate (EC) (1:1:1 by weight). All cells were assembled in the glovebox (Super, Mikrouna) under a high pure Ar atmosphere ($H_2O \leq 1$ ppm, $O_2 \leq 1$ ppm). Electrochemical tests were performed at a voltage of 2.0–3.8 V (vs Li/Li^+) using a battery test system (CT 4008, XINWEI). The cyclic voltammetry (CV) curves were measured on an electrochemical workstation (CHI660D, Shanghai Chen Hua Instrument Co. Ltd) in the range of 2.0–4.5 V at the same scan rate. The electrochemical impedance spectroscopy (EIS) data was acquired at 5 mV from 10 MHz to 1000 kHz. The research process is shown in Fig. 1.

Results and discussion

Effect of calcination temperature on the microstructure of regenerated $LiFePO_4$/C

Figure 2 shows the XRD patterns of regenerated $LiFePO_4$/C by pre-oxidation and reduction method at different temperatures (sucrose addition: 6%). The diffraction peaks of regenerated $LiFePO_4$/C were consistent with the diffraction peaks in JCPDS Card 81–1173, and there was no impurity peak. It indicated that $LiFePO_4$/C had been successfully regenerated by pre-oxidation and reduction method, and the regenerated materials had high purity and good crystallinity. Table 1 shows the ratio of diffraction peak intensity of regenerated $LiFePO_4$/C ((311) to (211), (111) and (101)). The intensity ratio of the diffraction peak of the crystal plane could be used to reflect the preferred growth orientation in the crystal growth process. As shown in Table 1, the regenerated $LiFePO_4$/C calcined at 600 ℃ mainly grew along the (111) and it mainly grew along the (311) when calcined at 700 ℃. The ratios of I(311)/I(211), I(311)/I(111), and I(311)/I(101) were all greater than 1, indicating that the preferred growth orientation of all materials was (311). It was consistent with the results in JCPDS Card 81–1173.

In Fig. 3, the agglomeration degree of regenerated $LiFePO_4$/C particles was low, and the particle size was about 2 μm. When calcined at 500–650 ℃, the regenerated

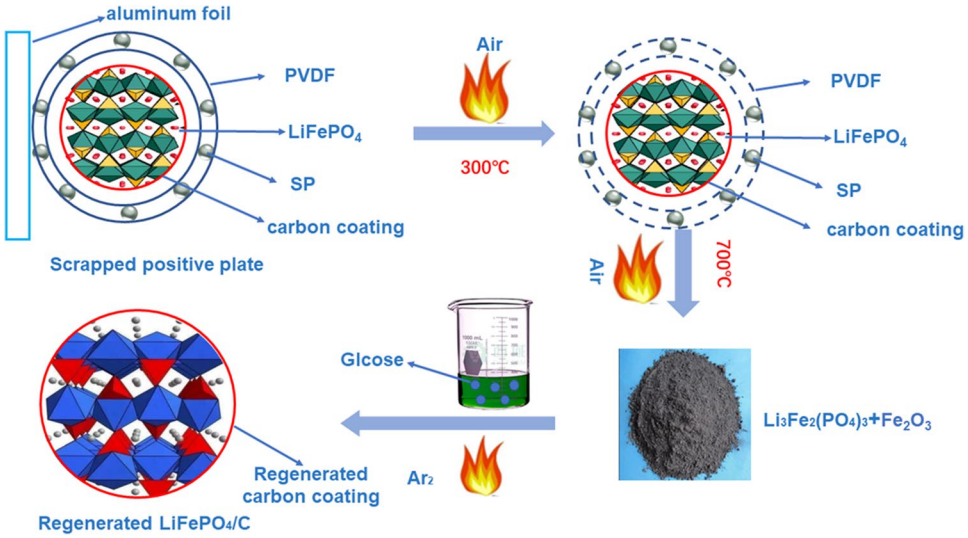

Fig. 1 Flow chart of research

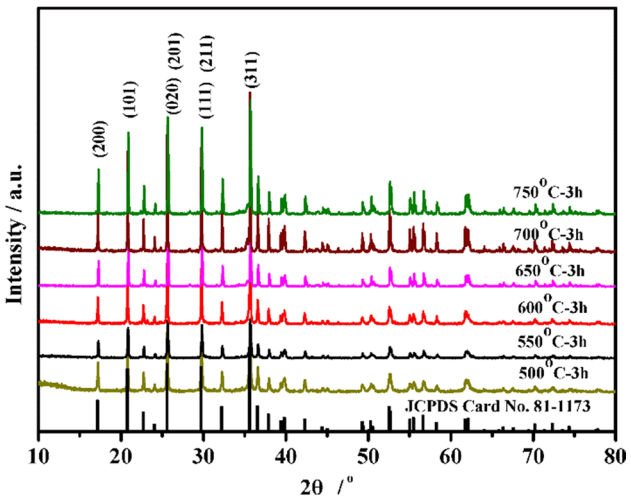

Fig. 2 XRD patterns of regeneration $LiFePO_4$/C

$LiFePO_4$/C particles were polygonal with poor consistency. It was mainly because the calcination temperature was low and the particles had not yet been globalized, so the particles remain in the original state. The amorphous carbon decomposed by sucrose could not be tightly coated around $LiFePO_4$/C particles, and the surface of the particles was rough (Fig. 3a–d). With the increase of calcination temperature (700–750 ℃), the particles gradually grew up and spheroidized obviously (Fig. 3e, f). Spherical particles with smaller particle size could improve the tap density and surface area of the cathode materials, which could improve the electrochemical performance of $LiFePO_4$/C. Therefore, 700 ℃ would be selected as the calcining temperature to study the influence of sucrose addition on the properties of regenerated $LiFePO_4$/C.

Effect of sucrose addition on the microstructure of regenerated $LiFePO_4$/C

During the synthesis of $LiFePO_4$, sucrose would provide a reducing atmosphere and form a surface coating. The low or higher carbon content in $LiFePO_4$/C was not conducive to improving the electrochemical performance of cathode materials, and it required to control the carbon content between 1.35 and 2.5%. Table 2 shows the carbon content of $LiFePO_4$/C regenerated by pre-oxidation and reduction method with different amounts of sucrose. With the increase of sucrose amounts, the residual amount of carbon in the regenerated $LiFePO_4$/C increased. When the sucrose addition was 9%, 10%, and 12% (marked 9%-RLFP, 10%-RLFP, 12%-RLFP), respectively, the carbon content was 1.41%, 1.59%, and 2.44%. Therefore, regenerated $LiFePO_4$/C with high sucrose addition was studied.

As shown in Fig. 4, with the increase of sucrose addition, the main phases were $LiFePO_4$/C and C. The regenerated $LiFePO_4$/C had a good crystal structure, and each diffraction peak corresponded to the diffraction peak in the JCDPS Card No.81–1173. When sucrose addition was 9%, impurity peak

Table 1 Intensity ratio of diffraction peaks of regenerated $LiFePO_4$/C

Intensity ratio	500℃-3 h	550℃-3 h	600℃-3 h	650℃-3 h	700℃-3 h	750℃-3 h	JCPDS card
I(311)/I(211)	1.176	1.178	1.127	1.224	1.523	1.319	1.267
I(311)/I(111)	1.089	1.045	1.018	1.114	1.255	1.177	1.215
I(311)/I(101)	1.227	1.290	1.206	1.387	1.584	1.394	1.314

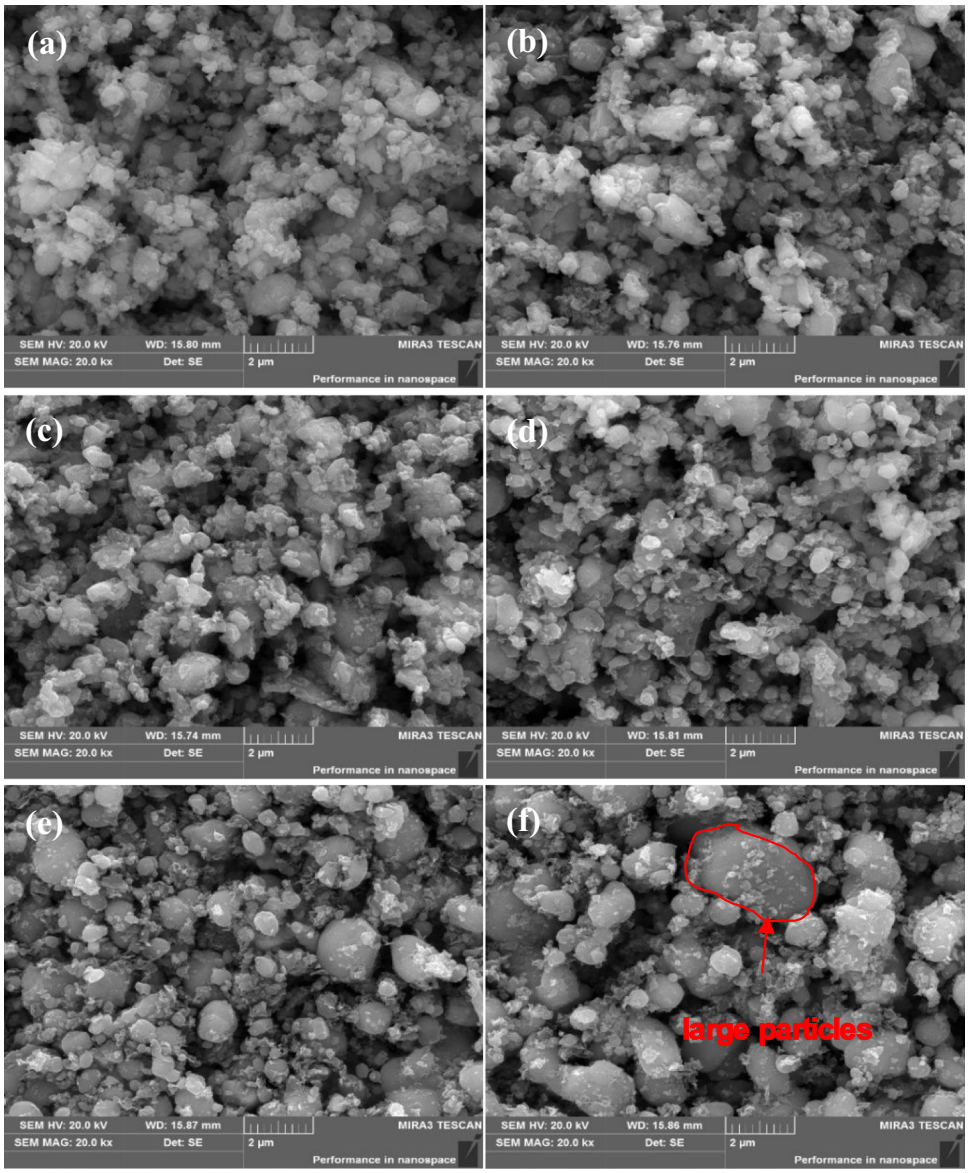

Fig. 3 SEM images of regeneration $LiFePO_4$/C at different temperatures (**a** 500℃-3 h, **b** 550℃-3 h, **c** 600℃-3 h, **d** 650℃-3 h, **e** 700℃-3 h, **f** 750℃-3 h)

Table 2 Contents of residual carbon in regenerated $LiFePO_4$/C with various sucrose additions

Sucrose addition /%	6	7	8	9	10	12
Carbon content /%	0.75	0.94	1.01	1.41	1.59	2.44

appeared in the regenerated sample. With low amount of sucrose, the reduction atmosphere generated at high temperature is weak and could not reduce Fe^{3+} completely to Fe^{2+}.

In Fig. 5, with the increase of sucrose addition, the number of fine particles and floccules between particles increased gradually. With higher sucrose addition (12%), the particle size of $LiFePO_4$ particles decreased, and some fine particles and floccules dispersed around the spherical particles or adhered to the surface of the particles. It might indicate that at high temperature, the carbon generated from the decomposition of sucrose around $LiFePO_4$ particles was preferentially coated on its surface (Fig. 8). The carbon far away from the $LiFePO_4$ particles was dispersed in the materials as granular or flocculent carbon. The carbon coating, granular or flocculent carbon prevented the sintering of $LiFePO_4$ and reduced the particle size of materials. Meanwhile, these different forms of carbon interweaved together to form a "strong" conductive network, shortening the diffusion path of Li^+, which improved the electrical conductivity of the materials.

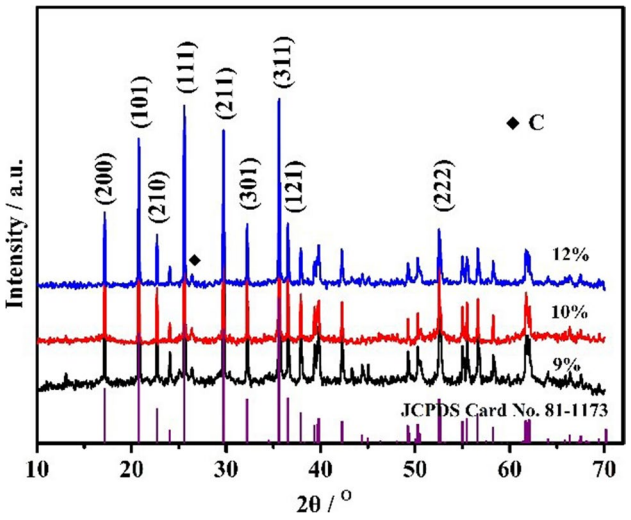

Fig. 4 XRD of regenerated $LiFePO_4$/C with different additions of sucrose

To further identify carbon coating on the surface of $LiFePO_4$, TEM tests were performed. Figure 6 shows the TEM images of regenerated $LiFePO_4$/C with different amounts of sucrose (9%, 10%, and 12%). With a lower sucrose addition (9% and 10%), the carbon coating of $LiFePO_4$ particles was discontinuous. As shown in Fig. 6a and b, the surface of $LiFePO_4$ was not completely coated. When the sucrose addition was 12%, the carbon coating was uniform and continuous, with a thickness of about 12–25 nm. Uniform coating was beneficial to improve the electrical conductivity of $LiFePO_4$ particles and improve the electrochemical performance of regenerated materials [21].

Electrochemical properties of regenerated $LiFePO_4$/C

Consequently, electrochemical tests were performed to investigate the performance variations between 9%-RLFP, 10%-RLFP, and 12%-RLFP. As shown in Fig. 7a, the charging specific capacity of 9%-RLFP, 10%-RLFP, and 12%-RLFP was 126.19, 138.33, and 148.92 mAh g^{-1}, and the discharging specific capacity was 118.85, 127.08, and 140 mAh g^{-1}, with the coulombic efficiency of 94.18%, 91.87%, and 94.01%, respectively. The 12%-RLFP had the highest charge–discharge ratio capacity. The charging and discharging voltage platform difference (ΔV) value of 12%-RLFP was smallest (Fig. 7b). This indicated that 12%-RLFP had high charge–discharge capacity, low polarization, and good reversibility. The conductive network composed of uniform carbon coating and amorphous (granular or flocculent) carbon improved the electrochemical performance of the regenerated materials.

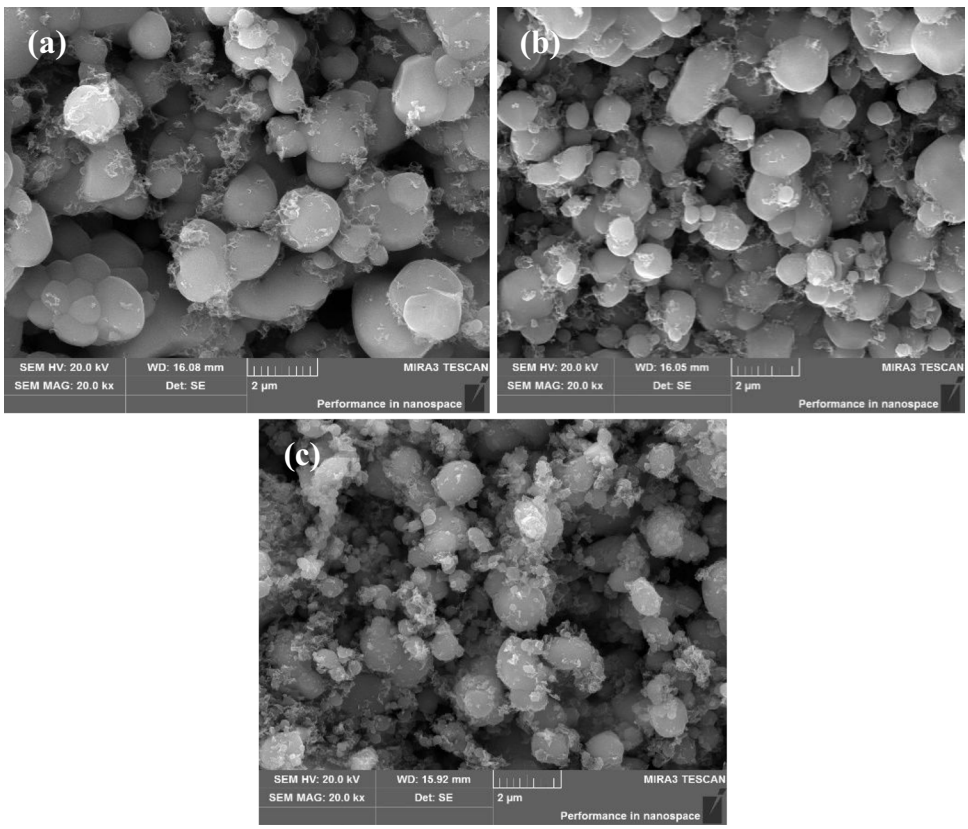

Fig. 5 SEM of regenerated $LiFePO_4$/C with different additions of sucrose (**a** 9%, **b** 10%, **c** 12%)

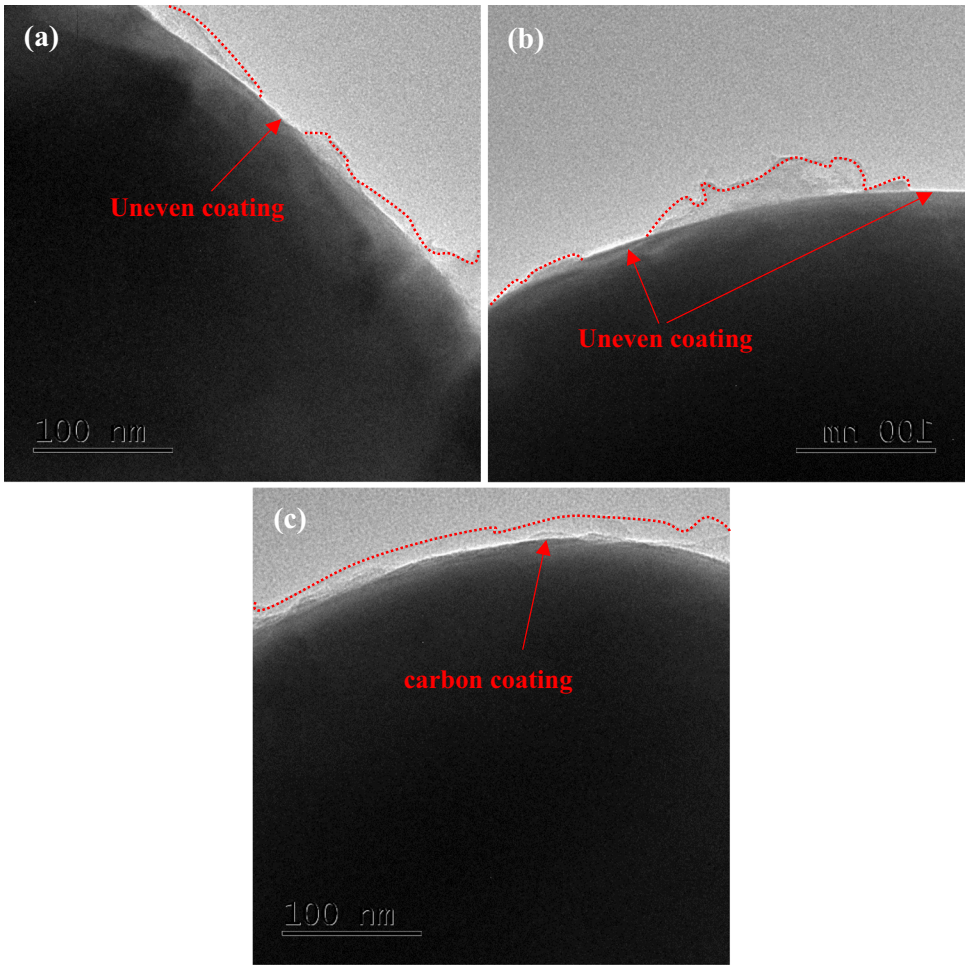

Fig. 6 TEM of regenerated $LiFePO_4/C$ with different additions of sucrose (**a** 9%, **b** 10%, **c** 12%)

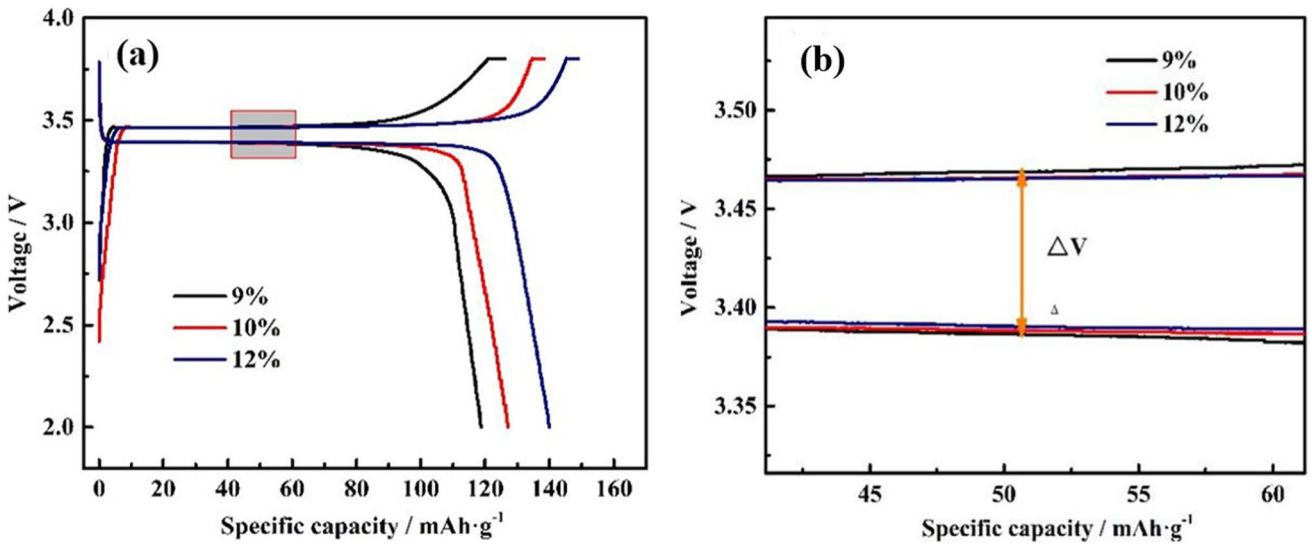

Fig. 7 **a** Initial charge–discharge curve at 0.1 C of regenerated $LiFePO_4/C$ (vs. Li/Li^+) with different additions of sucrose; **b** was partial enlarged detail of **a**

In Fig. 8, the rate performance of 12%-RLFP was excellent. When discharged at 4–10 C, the rate performance of 9%-RLFP was better than that of 10%-RLFP. At other discharge rates, 10%-RLFP had better performance than 9%-RLFP. According to the TEM, this special phenomenon might be caused by the inhomogeneity of carbon coating and the defects on the material surface.

The discharge specific capacity of regenerated $LiFePO_4$/C after 200 cycles at 0.5 C is shown in Fig. 8b. The values of 9%-RLFP, 10%-RLFP, and 12%-RLFP were 111.25, 120.21, and 135.51 mAh g^{-1} for the 200th cycle, respectively. And the capacity retention rate was 99.25%, 98.65%, and 99.80%, respectively. The excellent cycling performance of 12%-RLFP was mainly ascribed to the following reasons: (1) the uniform carbon coating on the surface of $LiFePO_4$ reduces the defects on the surface of particles and enhances the electrical conductivity; (2) the granular and flocculent carbon in the materials forms a bridge between $LiFePO_4$/C, which improved the electrical conductivity.

To determine the kinetic behavior of Li^+ transfer in the regenerated materials, the EIS results of the samples were compared (Fig. 9a). The EIS and the corresponding equivalent circuit of 9%-RLFP, 10%-RLFP, and 12%-RLFP within the scanning frequency range of 10 MHz–1000 kHz. EIS measurements were executed on the coin cell which had been cycled for 3 circles at 0.1 C. The fitting results of each electrode of the equivalent circuit in Fig. 9a are shown in Table 3. Fig. 9a displays the Nyquist plots of 9%-RLFP, 10%-RLFP, and 12%-RLFP samples. The profiles of 9%-RLFP, 10%-RLFP, and 12%-RLFP were composed of one semicircle at the high-frequency region and a straight line at the low-frequency region. Generally speaking, R_s and R_{ct} stand for electrolyte contact resistance and charge transfer resistance, respectively [22]. The R_s of 12%-RLFP (2.79 Ω) was higher than 9%-RLFP (5.66 Ω) and 10%-RLFP (4.25 Ω). The superior electrochemical performance of 12%-RLFP was primarily owing to its lower charge transfer resistance (73.71 Ω), which was affiliated with the Li^+ migration through the interface and charge–discharge resistance between the electrolyte and the surface of particles. Due to the higher carbon content and uniform coating of 12%-RLFP, the electrical conductivity of the regenerated material increased and the charge transfer resistance decreased, which follows that the results were consistent with the rate and cycling performances.

To further determine the Li^+ diffusion coefficient of the regenerated materials, the cyclic voltammetry curve of the regenerated material was tested. In Fig. 9b, the redox peak voltage differences of 9%-RLFP, 10%-RLFP, and 12%-RLFP were different (0.4 V, 0.39 V, and 0.38 V respectively), which was consistent with the change trend of the platform voltage difference of the first charge and discharge. The voltage difference of the redox peak could reflect the degree of reversibility of the electrochemical reaction. The voltage difference mainly depends on the conductivity of the material and the diffusion rate of Li^+ [15]. Therefore, 12%-RLFP had the higher Li^+ diffusion rate and higher electrical conductivity. Meanwhile the polarization of the sample was the smallest and the reversibility was the best. The diffusion coefficient of Li^+ can be calculated as shown in formula 1 [23].

$$i_{pc} = 0.4463(nF)^{3/2}(RT)^{-1/2}C_{Li^+}v^{1/2}AD^{1/2}{}_{Li^+} \quad (1)$$

where i_{pc} is peak current of cyclic voltammetry curve (A); N is charge transfer number (1); F is Faraday constant (96,485.33 C·mol^{-1}); R is perfect gas constant (8.314 J·mol^{-1}·K^{-1}); T is temperature (298.15 K); $C_{Li}{}^+$ is

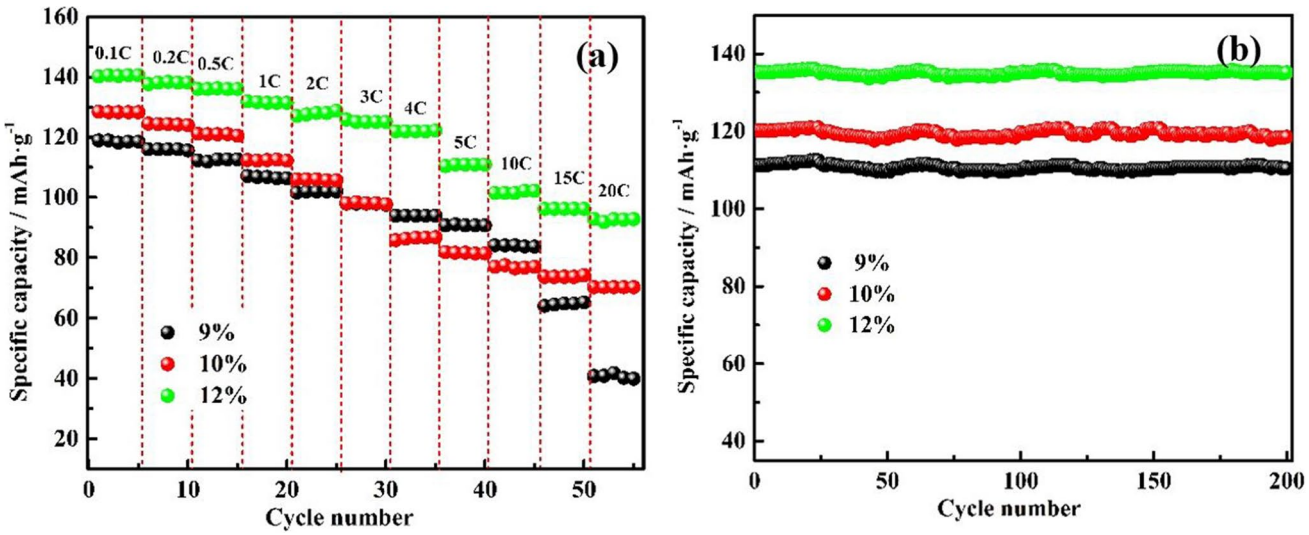

Fig. 8 **a** Rate capability and **b** cycling performance of regenerated $LiFePO_4$/C (vs. Li/Li^+) with different additions of sucrose

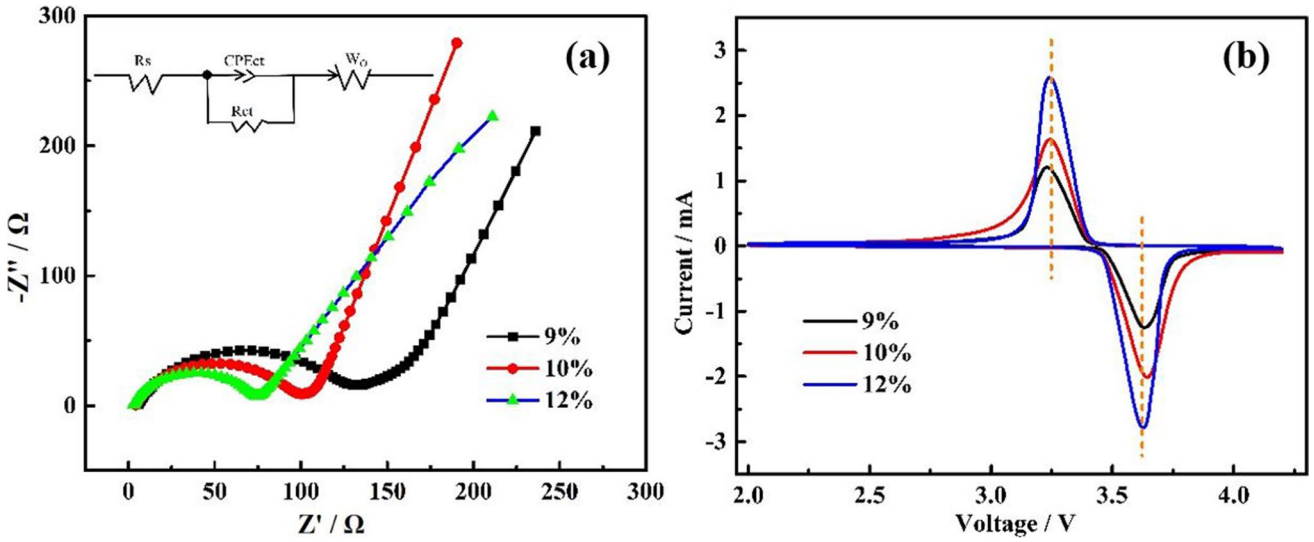

Fig. 9 **a** EIS of regenerated $LiFePO_4$/C (vs. Li/Li^+) with different additions of sucrose, **b** CV curves of regenerated $LiFePO_4$/C (vs. Li/Li^+) with different additions of sucrose in the voltage range of 2.0–4.2 V at the scan rate of 0.2 $mV{\cdot}s^{-1}$

Table 3 Fitting results of various anodes based on equivalent electric circuit from Fig. 9a

Sample	R_s (Ω)	R_{ct} (Ω)
9%	5.66	128.50
10%	4.25	95.93
12%	2.79	73.31

bulk ion concentration (0.0228 $mol{\cdot}cm^{-3}$); v is potential scanning rate (0.0002 $V{\cdot}s^{-1}$); A is effective electrode area (1.5386 cm^2); and D_{Li^+} is diffusion coefficient of lithium ion ($cm^2\ s^{-1}$).

The results show that the lithium-ion diffusion coefficients of 9%-RLFP, 10%-RLFP, and 12%-RLFP were $0.91e^{-5}$, $1.22e^{-5}$, and $1.94e^{-5}$ $cm^2{\cdot}s^{-1}$, respectively. The higher lithium-ion diffusion coefficient will improve the cycling performance and rate performance of the regenerated $LiFePO_4$/C, which was consistent with the test results in Fig. 8.

Conclusion

In this study, the scraped $LiFePO_4$/C was successfully regenerated at 500–750 ℃ by pre-oxidation and reduction method and the regenerated $LiFePO_4$/C had a spherical structure at 700 ℃. Regenerated $LiFePO_4$/C had good crystallinity. Sucrose decomposition products formed uniform carbon coating on 12%-RLFP surface. Carbon coating and granular-flocculent carbon conduction network enhance the electrical conductivity of regenerated materials. At 0.1 C, the voltage difference of 12%-RLFP discharge platform was the smallest with high reversibility. Meanwhile, the specific charging capacity and discharge capacity were 148.92mAh g^{-1} and 140mAh g^{-1}, respectively. The charge–discharge efficiency is 94.01%. 12%-RLFP has the highest lithium-ion diffusion coefficient ($1.94e^{-5}$ $cm^2\ s^{-1}$), and the excellent magnification and cycling properties are demonstrated. After 200 cycles, the capacity retention rate of 12%- RLFP was 99.80%.

Funding The authors acknowledge support from the Youth Foundation of Hunan Province (2021JJ40762), Natural Science Foundation of Hunan Province (2021JJ30794), and the Natural Science Foundation of China (Granted No. 2019YFC1907901-2).

Declarations

Conflict of interest The authors declare no competing interests.

References

1. Chu S, Cui Yi, Liu N (2016) The path towards sustainable energy[J]. Nat Mater 16:16–22
2. Thackeray MM, Wolverton C, Isaacs ED (2012) Electrical energy storage for transportation-approaching the limits of, and going beyond, lithium-ion batteries[J]. Energy Environ Sci 5:7854–7863
3. Vinodkumar E, Rotem M, Ran E et al (2011) Challenges in the development of advanced Li-ion batteries: a review[J]. Energy Environ Sci 4:3243–3262
4. Goodenough JB, Kim Y (2010) Challenges for rechargeable Li batteries[J]. Chem Mater 22:587–603
5. Zubi G, Dufo-López R, Carvalho M et al (2018) The lithium-ion battery: state of the art and future perspectives[J]. Renew Sust Energ Rev 89:292–308
6. Harper G, Sommerville R, Kendrick E et al (2019) Recycling lithium-ion batteries from electric vehicles[J]. Nature 575(7781):75–86

7. Xiaohong Zheng, Zewen Zhu, XiaoLin, et al. (2018) A mini-review on metal recycling from spent lithium-ion batteries[J]. Engineering, 4(3): 361–370.
8. Jinqiu Xu, Thomas Hywel Rhys, Francis Robert W et al (2008) A review of processes and technologies for the recycling of lithium-ion secondary batteries[J]. J. Power Sources 177:512–527
9. Fan E, Li Li, Zhang X et al (2018) Selective recovery of Li and Fe from spent lithium-ion batteries by an environmentally friendly mechanochemical approach[J]. ACS Sustainable Chem Eng 6(8):11029–11035
10. Yang Y, Zheng X, Cao H et al (2017) A closed-loop process for selective metal recovery from spent lithium iron phosphate batteries through mechanochemical activation[J]. ACS Sustainable Chem Eng 5(11):9972–9980
11. Li H, Xing S, Liu Y et al (2017) Recovery of lithium, iron, and phosphorus from spent $LiFePO_4$ batteries using stoichiometric sulfuric acid leaching system[J]. ACS Sustainable Chem Eng 5(9):8017–8024
12. Yongzhi C, Lihua W et al (2020) Preparation of $FePO_4$ and LiH_2PO_4 from cathode mixture materials of scrapped $LiFePO_4$ batteries[J]. J Mater Sc-Mater El 31(5):4083–4091
13. Zhang J, Juntao Hu, Liu Y et al (2019) Sustainable and facile method for the selective recovery of lithium from cathode scrap of spent $LiFePO_4$ batteries[J]. ACS Sustainable Chem Eng 7(6):5626–5631
14. Liu K, Tan Q, Liu L et al (2019) Acid-free and selective extraction of Lithium from spent lithium iron phosphate batteries via a mechanochemically induced isomorphic substitution[J]. Environ Sci Technol 53(16):9781–9788
15. Wang L, Li J, Zhou H et al (2018) Regenerating cathode material mixture from spent lithium iron phosphate batteries[J]. J Mater Sc-Mater El 29(11):9283–9290
16. Li J, Wang Ya, Wang L et al (2019) A facile recycling and regeneration process for spent $LiFePO_4$ batteries[J]. J Mater Sc-Mater El 30(15):14580–14588
17. Li X, Zhang J, Song D et al (2017) Direct regeneration of recycled cathode material mixture from scrapped LiFePO4 batteries[J]. J Power Sources 345:78–84
18. Chen J, Li Q, Song J et al (2016) Environmentally friendly recycling and effective repairing of cathode powders from spent $LiFePO_4$ batteries[J]. Green Chem 18:2500–2506
19. Yang Y, Zheng X, Cao H et al (2017) A closed-loop process for selective metal recovery from spent lithium iron phosphate batteries through mechanochemical activation[J]. ACS Sustain Chem Eng 5:9972–9980
20. Zheng R, Zhao Li, Wang W et al (2016) Optimized Li and Fe recovery from spent lithiumion batteries via a solution-precipitation method[J]. RSC Adv 6:43613–43625
21. Huang Y, Zheng F, Zhang X et al (2014) Effect of carbon coating on cycle performance of $LiFePO_4$/C composite cathodes using Tween80 as carbon source[J]. Electrochim Acta 130:740–747
22. Zhou Hongming, Zhao Xiuxiu, Yin Chengjie et al (2018) Regeneration of $LiNi_{0.5}Co_{0.2}Mn_{0.3}O_2$ cathode material from spent lithium-ion batteries[J]. Electrochim. Acta 291:142–150
23. Li S, Thomas A (2020) Advanced nanomaterials for electrochemical-based energy conversion and storage[M]. Micro and Nano Technologies